A smeared seismicity constitutive model

A. Ord[1], B. E. Hobbs[1], and K. Regenauer-Lieb[1,2]

[1]*Predictive Mineral Discovery Cooperative Research Centre, CSIRO Exploration and Mining, PO Box 1130, Bentley, WA 6102, Australia*
[2]*Johannes Gutenberg-Universitat Mainz, Geophysics and Geodynamics, 55099 Mainz, Germany*

The classical application of rate and state dependent frictional constitutive laws has involved the instabilities developed between two sliding surfaces. In such a situation, the behaviour and evolution of asperities is the controlling mechanism of velocity weakening. However, most faults have a substantial thickness and it would appear that it is the bulk behaviour of the fault gouge, at whatever scale, that is important. The purpose of this paper is to explore how bulk frictional sliding behaviour may be described. We explore here the consequences of applying the rate and state framework initially developed to describe the frictional behaviour at the interface between two interacting sliding blocks, to frictional behaviour within a layer of gouge that has bulk elastic-plastic constitutive behaviour. The approach taken here is to replace the relative sliding velocity in the classical formulation with the maximum shear strain rate, D, and the characteristic length with a characteristic shear strain, γ_c. This means that the frictional behaviour of the bulk material now evolves with shear strain rate, D, over a characteristic shear strain, γ_c. This approach still does not address the problem of reproducing natural recurrence times between instabilities, but perhaps places the problem in a new framework.
Key words: Seismicity, constitutive model, rate and state dependant friction, bulk frictional elastic-plastic behaviour.

1. Introduction

Understanding the seismic behaviour of large faults involves studies at a range of length scales (see Fig. 1). At the finest length scale one is concerned with the behaviour of asperities at grain or fracture contacts. Here the micromechanical properties of the asperities are fundamental, and friction (Dieterich, 1979), crystal-plastic (Bowden and Tabor, 1950; Estrin and Brechet, 1996) or melting (Hirose and Shimamoto, 2004) processes are paramount. At this scale, discontinuum computational procedures are appropriate. At centimetre to kilometre scales, commonly the issue may concern the behaviour of fault gouge or of mylonitic material. Here the constitutive behaviour of the bulk fault filling material is the point of interest and continuum computational procedures are appropriate; this is the focus of this paper. At larger scales, various combinations of discontinuum and continuum schemes may be appropriate until, at the largest scales (that of the crust and mantle), continuum codes involving coupling of various elastic, plastic and viscous constitutive behaviours may be appropriate (see Iio *et al.*, 2004). As always in such multiscaling problems, the challenge is to develop an overarching strategy that enables 'handshaking' between the various scales. Such a strategy probably involves a thermodynamic approach where the dissipation of Helmholtz free energy is tracked across the scales (see Lavenda, 1978) but this has not yet been fully developed for the seismic problem although progress exists in other geoscience areas

(Regenauer-Lieb and Yuen, 2004). Moreover, such an approach, based on non-equilibrium thermodynamics, is made more appealing by the experimental demonstration (Hirose and Shimamoto, 2004) that melting may be an important part of the seismic instability process. As indicated, the emphasis here is on that scale where a continuum description of the seismic process is appropriate, and our emphasis is on plastic rather than thermal-viscous behaviour as may be relevant to production of melt or to the bulk behaviour of mylonites.

Experimental studies since Leonardo da Vinci (MacCurdy, 1938) have confirmed that, to first-order, the frictional shear stress τ between two sliding blocks is linearly related to the normal stress σ_N. This relationship, $\tau = \mu\sigma_N$, where μ is a constant known as the coefficient of friction, is commonly referred to as Amontons' Law (Amontons, 1699). Gu *et al.* (1984) have pointed out that it is the second order departures from Amontons' Law that may govern whether frictional sliding is stable or not. These departures from Amontons' Law, which involve a dependence of μ upon both the velocity of sliding and upon the evolution of the state of the sliding interfaces, lead to stability criteria for sliding with new rock friction constitutive relations and have important implications for earthquake mechanics.

However, real faults in the upper half of the crust commonly have a finite thickness and are comprised of a zone of crushed rock particles or gouge. It appears that it is the mechanical behaviour of this fault gouge that is important in controlling the unstable sliding behaviour of many faults rather than the frictional behaviour and the evolution of the state of the discrete fault surfaces themselves. Of course, it may be, in making such a statement, that the problem
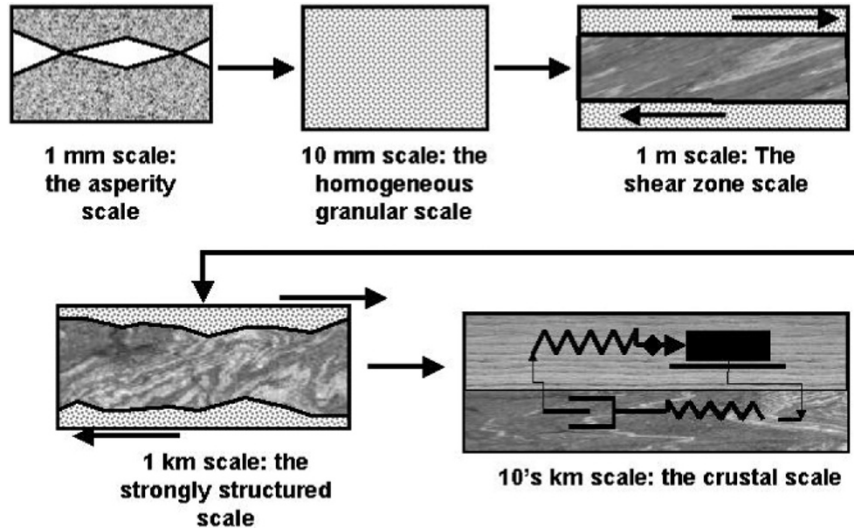
Fig. 1. The multiscaling seismic problem. At the 1 mm scale, discontinuum mechanics is relevant. At the 10 mm to 1 km scale, continuum mechanics may be more relevant, whilst at the crustal scale, coupled continuum models, as developed by Iio *et al.* (2004), may be a better representation of the mechanics.

has simply been shifted to another scale, namely that of the individual gouge particles, or that the unstable behaviour is now developed upon a new surface that is propagated within the gouge itself. The problem here is again emphasised by Fig. 1; laboratory experiments are performed at the 1 mm to 10 mm scale, earthquakes occur within a crustal scale system, and the geologist observes at the 1 m to 1 km scale. Whatever is the mechanism for unstable behaviour at the scale of the gouge layer, it seems profitable to explore a "smeared" representation of the gouge layer by representing the gouge as a material with frictional constitutive behaviour, that is, the bulk constitutive behaviour is dependent upon the normal stress across any plane within it, or, as we will develop, the first invariant of the deviatoric stress tensor, but with the added characteristic that the frictional behaviour is also weakly dependent upon the shear strain rate and upon parameters that describe the evolution of the state of the gouge, and that evolve over a characteristic shear strain. In order for this bulk constitutive behaviour to be invariant with respect to coordinate transformations, it is necessary to express the constitutive laws in terms of stress, strain, and strain-rate invariants. This is the approach taken here so that the stress drop associated with an instability, and the shear strain rate, are expressed as second invariants of the respective deviatoric tensor.

This paper explores such behaviour within the framework of a non-associative, Mohr-Coulomb constitutive law (see Vermeer and de Borst, 1984) for the bulk behaviour of the gouge. We show that this approach enables bulk frictional instabilities to be modelled. An additional advantage is that this constitutive behaviour leads to the spontaneous development of localised shear zones within the deforming gouge as has been described by Marone (1998), allowing the relation of unstable behaviour to the development of these shear zones to be investigated in the future.

Elastic-plastic bulk constitutive relations other than Mohr-Coulomb are possible, of course, including Drucker-Prager constitutive behaviour and a range of other be-

haviours transitional between Drucker-Prager and Mohr-Coulomb (see Borja and Aydin, 2004); however, Drucker-Prager seems to be more relevant to weak soils or clays. The Mohr-Coulomb behaviour is explored here because, of all the elastic-plastic bulk constitutive relations, the presence of corners on the yield surface means that localisation, or shear zone development, is favoured, even for an associative material (see Besuelle and Rudnicki, 2004).

Here we fuse two empirical approaches: a robust criterion for the failure of bulk material (the Mohr-Coulomb plasticity model), and a generalisation of a laboratory derived evolution equation for the frictional behaviour of brittle surfaces (the rate and state variable friction approach).

1.1 Bulk frictional elastic-plastic behaviour

Deforming materials, which display frictional behaviour, expressed as a dependence on pressure or on normal stress, may be described by a plasticity model such as the *Mohr-Coulomb plasticity* model, which is used to describe bulk materials that yield when subjected to shear loading. The constitutive parameters (see Vermeer and de Borst, 1984) are the cohesion, c, the friction angle, ϕ, the tensile strength, and the dilation angle, ψ. In addition, two elastic constants are required for an isotropic elastic-plastic material; here we employ the shear and bulk elastic moduli.

We use the Mohr-Coulomb yield function

$$f^S = \sigma_1 - \sigma_3 N_\phi + 2c\sqrt{N_\phi} \qquad (1)$$

where ϕ is the friction angle, c, the cohesion, and

$$N_\phi = (1 + \sin\phi)/(1 - \sin\phi) \qquad (2)$$

The shear potential function g^s for (irreversible) plastic deformation, corresponds to a non-associated flow rule and has the form

$$g^s = \sigma_1 - \sigma_3 N_\psi \qquad (3)$$

where ψ is the dilation angle and

$$N_\psi = (1 + \sin\psi)/(1 - \sin\psi) \qquad (4)$$

Throughout we consider only plane strain, and take the principal stresses in the plane of deformation to be σ_1 and σ_3 with $|\sigma_1| > |\sigma_3|$ and compression negative.

Shear dilatancy, or dilatancy, is the change in volume that occurs with shear distortion of a material. In a Mohr-Coulomb material, for (irreversible) plastic deformation, dilatancy is characterized by a dilation angle, ψ, which is related to the ratio of plastic volume change to plastic shear strain. This angle can be specified in the Mohr-Coulomb plasticity model (see Vermeer and de Borst, 1984) and is found from a plot of volumetric strain versus axial strain determined for triaxial tests or shear box tests. The initial slope for this plot corresponds to the elastic regime, while the slope used to measure the dilation angle corresponds to the plastic regime (see Ord, 1991, for examples of the derivation of this and other Mohr-Coulomb constitutive parameters for sandstone and marble).

These are the criteria which describe the conditions for failure, or yield, of an elastic-plastic Mohr-Coulomb material. Until the critical yield stress is reached, the material is elastic, and any deformation is reversible. On yield, the material may undergo irreversible or plastic deformation, and the material behaviour during such plastic deformation is described by the plastic potential g^s or the flow rule which defines the orientation of the incremental plastic strain-rate vector for an imposed stress state. This incremental strain rate vector is always normal to the potential surface defined by Eq. (3). If this vector is also normal to the yield surface defined by Eq. (1), (i.e. $\phi = \psi$), then the constitutive behaviour is associative; otherwise it is non-associative. In the models explored here, the shear flow rule is non-associated and the tensile flow rule is associated.

Bifurcation, or a departure from homogeneous to inhomogeneous behaviour, is allowed in such a plasticity model so long as the dilation angle does not equal the friction angle; such material is called non-associative. Non-associated Mohr-Coulomb materials can therefore localise at yield (i.e. families of discontinuities such as shear bands develop in a material that starts as a homogeneous continuum). However, as implied above, Mohr-Coulomb materials can also localize when the stress state corresponds to a corner on the yield surface (see Besuelle and Rudnicki, 2004). This corresponds to stress states such as exist in axisymmetric compression or extension.

In this paper we generalise the rate and state approach to frictional sliding of a single block to apply to deformation of cataclastic fault gouge by writing the evolution equations in terms of the second invariants of the stress and strain rate tensors within the framework of an elastic-plastic Mohr-Coulomb material. As such, the frictional response of the bulk gouge depends upon the pressure within the material rather than the normal stress across a single sliding surface. This is expressed as a conical *yield surface* in stress space with a hexagonal cross section that expands in stress space in the direction of the hydrostatic stress axis. The opening angle of this cone is related to the angle of friction of the material. Excellent discussions of this concept are given by Borja and Aydin (2004), and by Besuelle and Rudnicki (2004). The conventional expression of the Mohr-Coulomb relationship is $\tau = c + \mu \sigma_N$ where τ is the shear stress on a plane with normal stress σ_N, c is the cohesion and μ is the coefficient of friction equal to $\tan \phi$ where ϕ is the angle of friction. A way of writing this expression as a yield criterion is $f = \tau - c + \mu \sigma_N$. Then, if $f = 0$ the material is at yield and if $f < 0$ then the material is elastic. Equation (1) is the identical expression for f written in terms of the principal stresses rather than in terms of τ and σ_N.

An additional intrinsic part of the formulation of these constitutive properties is the existence of another conical surface, namely, the *potential surface*, now existing in strain rate space. This also is hexagonal in cross section for a Mohr-Coulomb material but the opening angle of this cone is related to the angle of dilation. The importance of the potential surface is that the incremental strain rate vector is normal to this surface and not the yield surface. Thus the potential surface defines the deformation of the material whereas the yield surface defines the stress state. The potential surface defines the flow rule for the material whereas the yield surface defines whether the material is at yield or elastic for a prescribed stress state. These concepts as well as the theory are discussed by Vermeer and de Borst, 1984. Whereas the sliding direction of a single interface between two pieces of rock is defined by the geometry of the system plus the imposed forces, the bulk deformation of an elastic-plastic material requires the definition of both the yield surface and the potential surface together with the imposed stress or velocity field.

As we have indicated, Eqs. (3) and (4) define the potential surface in shear strain rate space, and hence in turn define the increment of plastic shear strain once the stress state is defined by Eqs. (1) and (2). This is equivalent to solving the partial differential equations known as the *flow rule*.

Briefly, the flow rule is expressed as:

$$\Delta \varepsilon_i^p = \gamma^\varepsilon \partial g_i^s / \partial \sigma_i \qquad i = 1, 3 \qquad (5)$$

where $\Delta \varepsilon_i^p$ are the principal incremental plastic strains, g^s is the potential function given in Eq. (3), and σ_i are the principal stresses. The constant λ^s is obtained in each increment of deformation by requiring that the new stress at the end of the increment be located on the yield surface given in Eq. (1).

After considerable manipulation, one obtains:

$$\lambda^s = f^s(\sigma_1^I, \sigma_3^I) / \left\{ (\alpha_1 - \alpha_2 N_\psi) - (\alpha_2 - \alpha_1 N_\phi) N_\phi \right\} \quad (6)$$

The superscript I refers to a new stress obtained by adding an increment of elastic stress to the old stress that existed at the beginning of the increment given the requirement that the new stress state lies on the yield surface. α_1 and α_2 are functions of both the elastic shear and bulk moduli and N_φ, N_ψ are as given in Eqs. (2) and (4). Thus the implementation of the flow rule requires the use of Eqs. (1), (2), (3) and (4). This explanation is quite condensed. For more insight one should examine Vermeer and de Borst or better, the FLAC user's manual (ITASCA, 2002; and see Appendix A) to get a true appreciation of the process involved. Similar discussions can be found in the textbook by Malvern (1969) but in this case, the theory is applied only to associated plastic materials where the yield and potential surfaces are coincident.
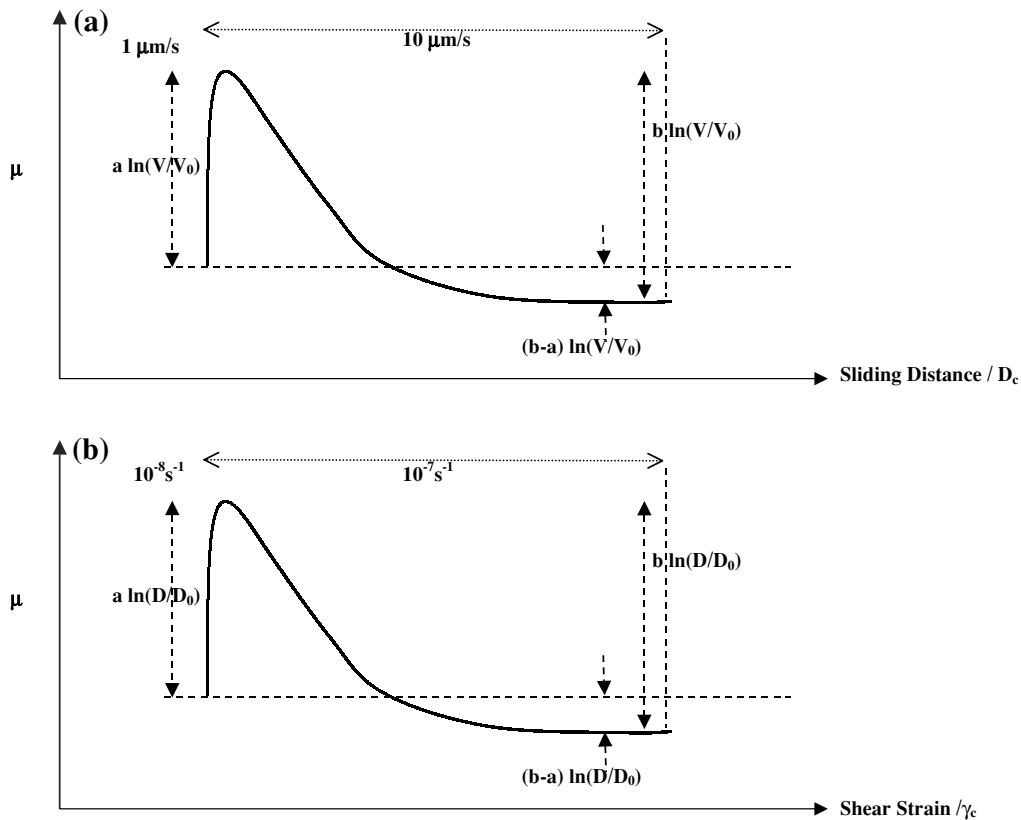
Fig. 2. a) Representation of the behaviour of the friction coefficient for velocity weakening behaviour (from Marone, 1998). b) Representation of the behaviour of the friction coefficient for shear strain weakening behaviour, as developed in this paper.

1.2   Rate and state dependent frictional behaviour

Experimental studies on frictional sliding between two surfaces as performed and interpreted by Dieterich (1978, 1979) and by Ruina (1980, 1983) have led to a constitutive relation which describes shear stress τ at constant normal stress σ_N to be dependent on the relative slip velocity V and the prior slip history in the form of dependence on a set of phenomenological parameters called state variables (θ_i). The state variables describe the state of the sliding surface and they evolve, as the surface slides, with a set of characteristic lengths D_{ci}.

The general forms of these relations as given by Ruina are:

$$\tau = F(V, \sigma_N, \theta_1, \theta_2, \ldots \theta_m) \tag{7}$$

$$\frac{d\theta_i}{dt} = G_i(V, \sigma_N, \theta_1, \theta_2, \ldots \theta_m) \qquad i = 1, m \tag{8}$$

During slip at a fixed slip rate and normal stress, the state variables evolve toward steady-state values θ_i^{ss} such that the shear stress evolves towards a steady-state value of $\tau^{ss}(V)$ corresponding to the imposed fixed speed and normal stress. The evolution of the coefficient of friction following a perturbation in the sliding velocity is shown in Fig. 2(a); here the behaviour is that of velocity weakening so that an increase in sliding velocity leads ultimately to a decrease in the friction coefficient.

However, although such rate and state behaviour is commonly attributed to frictional evolution between two sliding surfaces, identical behaviour is also observed when a layer of gouge is intentionally placed between two sliding blocks

(see Marone, 1998, for a discussion). Thus, in extending the relations given in Eqs. (7) and (8) to the situation where significant thicknesses of gouge are present, it seems profitable to explore the results of generalising these equations so that the frictional evolution is expressed in terms of continuum parameters such as strain rate and strain rather than the discontinuum parameters, V and D_c.

Equations (7) and (8) can be thought of as a discontinuum formulation of the evolution of friction as two blocks move with a relative velocity, V, parallel to the interface between them. The generalisation of such equations to develop a frame invariant constitutive relation that describes the evolution of friction in a continuum means that the evolution needs to be formulated in terms of invariants of the strain and strain-rate tensors. Moreover, since the deformational response is strongly non-linear, the incremental forms of the constitutive relations are relevant. Thus, instead of the characteristic distance, D_c, which is used in the discontinuum description to describe the spatial scale for frictional evolution (see Fig. 2(a)), we use a characteristic shear strain, γ_c.

Similarly, instead of the velocity, V, we use the maximum shear strain-rate, D, which is the square root of the second invariant of the incremental strain rate deviator tensor. We can then write:

$$\tau = F(D, \sigma_N, \theta_1, \theta_2, \ldots \theta_m) \tag{9}$$

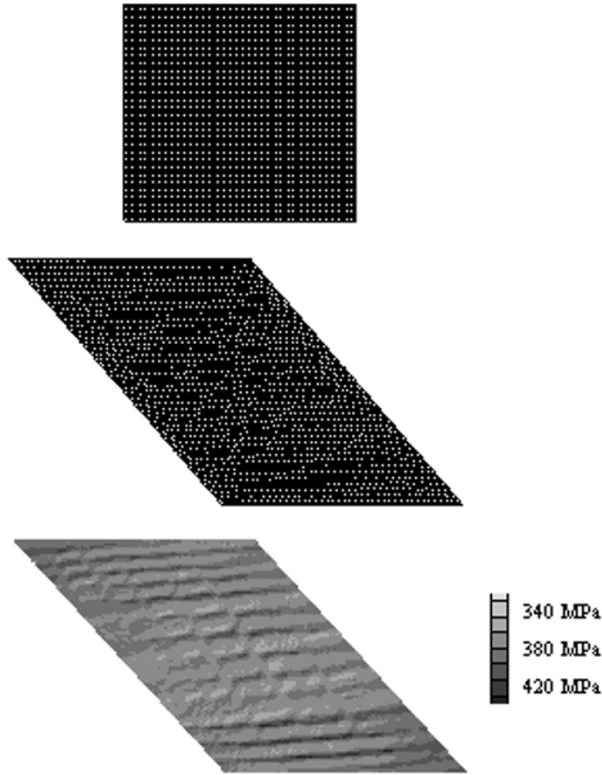$$\frac{d\theta_i}{dt} = G_i(D, \sigma_N, \theta_1, \theta_2, \ldots \theta_m) \qquad i = 1, m \tag{10}$$

Table 1. Mechanical properties for the simple shearing model.

Mechanical Property		
bulk modulus	47.0	GPa
shear modulus	28.0	GPa
density	2700	kg.m^{-3}
friction angle	30.0	degrees
dilation angle	1.0	degrees
cohesion	20.0	MPa
tensile strength	2.0	MPa

Table 2. Values for parameters in Eqs. (11), (12) and (13).

Parameter		
reference maximum shear strain rate D_o	1×10^{-3}	s^{-1}
characteristic shear strain γ_c	2×10^{-2}	
b	0.008	
a	0.006	
$a - b$	-0.002	
steady state friction, μ_O, at reference maximum shear strain rate	25	degrees

Fig. 3. a) Undeformed state of numerical grid. b) Deformed numerical grid. c) Contours of shear stress. Note that the conjugate set of shear bands is developed locally. Localities of histories shown in Fig. 4 are plotted as X, Y, and Z.

In Eqs. (9) and (10), σ_N should now be thought of as the first invariant of the deviatoric stress tensor, $(\sigma_{11} + \sigma_{22} + \sigma_{33})/3$.

In this paper we explore the effect of applying this kind of frictional behaviour to the evolution of the friction angle in the Mohr-Coulomb constitutive relation during a seismic event. The implication here is that the variables θ_i are state variables of the gouge, and that these evolve over a characteristic shear strain as the gouge deforms, with a dependence on the local shear strain rate, as shown in Fig. 2(b), now replacing Fig. 2(a). Throughout this paper from now on, we refer to the square root of the second invariant of the deviatoric stress tensor as the *shear stress* and the square root of the second invariant of the incremental deviatoric strain rate tensor as the *shear strain rate*.

The rate and state dependant behaviour is formulated in this instance as a single state variable law (i.e. $m = 1$ in Eqs. (9) and (10)):

$$\mu = \mu_O + a \ln(D/D_O) + b(\xi) \qquad (11)$$

where

$$d\xi/dt = -(\xi + \ln(D/D_O)D/\gamma_c. \qquad (12)$$

μ is the current friction coefficient, μ_O a reference friction coefficient, D the maximum shear strain rate at a point in the continuum where μ is measured, D_O a reference material maximum shear strain rate where μ_0 is measured, a and b are constitutive variables, ξ is the state variable, and γ_c is a characteristic shear strain scaling the evolution of the state variable.

In order now to apply this constitutive framework to a bulk material rather than a discrete sliding surface, we assume that ϕ, the friction angle included in the Mohr-Coulomb plasticity model, may be replaced by arctan μ, where μ is the friction coefficient involved in the rate and state variable behaviour. The explicit behaviour of a single sliding surface is in this way replaced by a smeared bulk description of the bulk material. This represents a multi-scaling from a distinct element description to a continuum description of the same problem on a larger scale. The approach is similar to that of Lyakhovsky (2001; Lyakhovsky *et al.*, 2001) who treat the incorporation of damage mechanics into a continuum code. In the formulation used here, the state variable ξ is updated in each time step according to

$$\xi_{new} = \xi_{old} - (\xi_{old} + \ln(D/D_o))(D/\gamma_c)\Delta t \qquad (13)$$

where Δt is the time step, which is calculated while the experiment is stepping numerically. The resulting friction coefficient, updated through Eq. (11), is then returned to the bulk Mohr-Coulomb constitutive behaviour through updating the friction angle.

In summary, our approach is to consider a non-associated Mohr-Coulomb material as our primary material. This is modified by specifying that the friction in the Mohr-Coulomb constitutive model evolves with shear strain in a manner analogous to rate and state dependent friction laws. The dilation angle is also included in such a constitutive formulation but we let it remain constant. Although there have been suggestions (particularly by Marone, 1998) that evolution of dilatancy may be important for real fault behaviour we have not explored evolution of dilatancy in this paper since it would add even greater complexity.
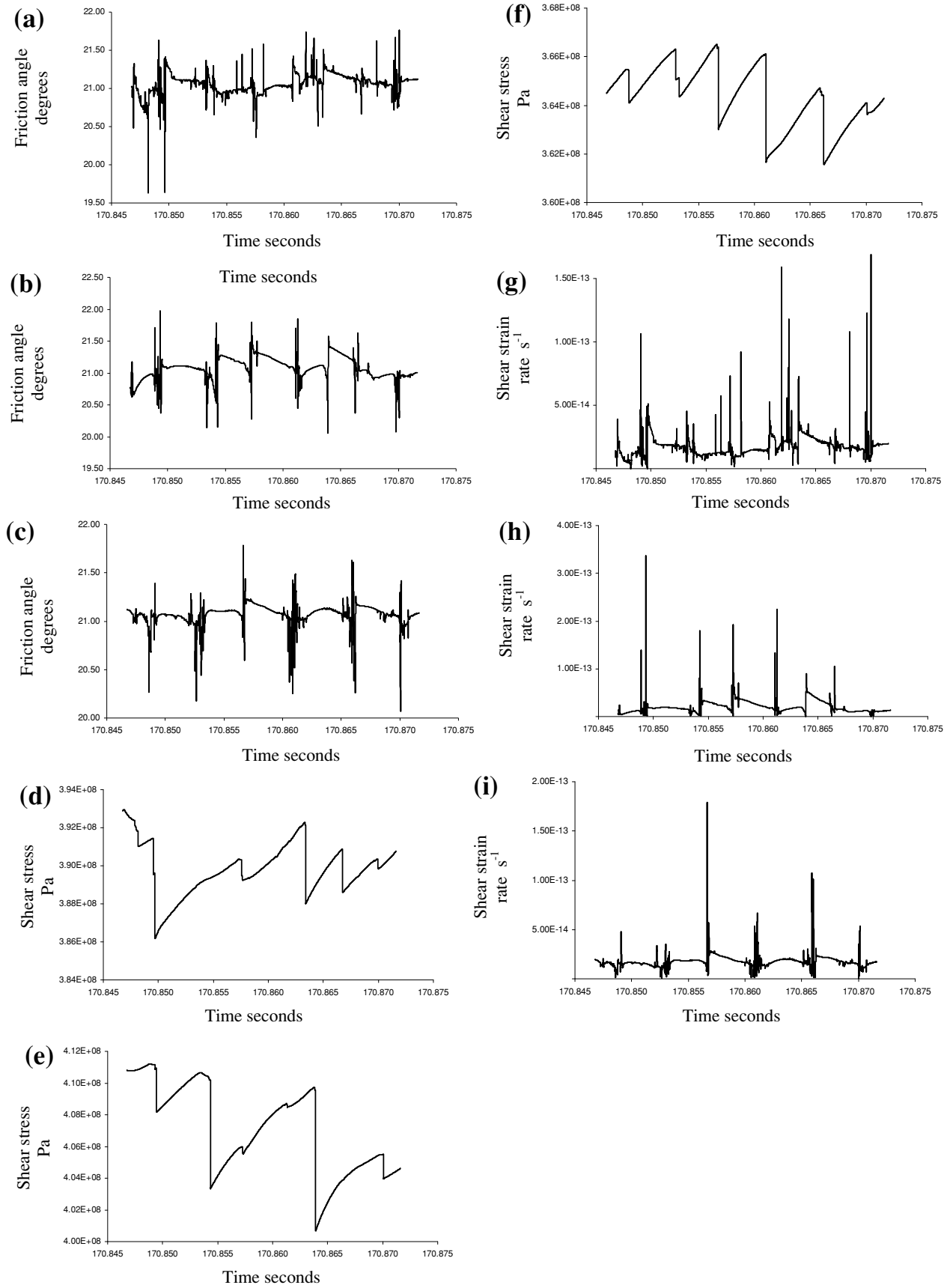
Fig. 4. Behaviour over 0.3 seconds for the three zones shown in Fig. 3(c), in the simple shearing model. (a), (b), (c): Friction angle versus time. (d), (e), (f): Shear stress versus time. (g), (h), (i): Shear strain rate versus time. (a), (d), (g): Position X in Fig. 3(c). (b), (e), (h): Position Y in Fig. 3(c). (c), (f), (i): Position Z in Fig. 3(c).

2. A Small Scale Model

2.1 Geological description

The development of structure in the form of shear bands within the deforming gouge of the fault zone is documented by various authors (see Marone, 1998, for a review). Such localisation introduces another spatial scale, other than γ_c, into the structural evolution of the material. The smeared approach adopted in this paper now allows us to investigate the evolution of instabilities during the development of such structures, building on earlier work exploring the initiation and development of shear zones and their patterning within an elastic-plastic (Mohr-Coulomb) material (Ord, 1991). One should note here that shear bands form spontaneously at yield in non-associative elastic-plastic materials or in elastic-plastic materials with corners on the yield surface (see Besuelle and Rudnicki, 2004, for a discussion). The spacing of the shear bands here depends on the grid size used since there is no internal length scale incorporated within the Mohr-Coulomb constitutive law.

2.2 Computational model

This square model, 75 metres on edge (75×75 computational zones), is shown in plan view in the undeformed state in Fig. 3(a); gravity is not turned on. The mechanical properties of the model are as in Table 1.

Velocity boundary conditions are imposed which result in isochoric bulk simple shearing. Rate and state variable dependant behaviour is imposed, with properties as in Table 2.

As described above, the classical rate and state formulation is specifically for a sliding surface, for unstable behaviour along a discontinuity. We choose here that this remains a critical behaviour at grain scale, and we scale up to a continuum formulation for a shear zone by assuming that the arc tan of the friction coefficient μ, may be used as the friction angle ϕ in the Mohr-Coulomb plasticity model. Variations in the magnitude of D_c, as determined by theory and by laboratory and field observations, are discussed by Marone (1998). In this study, we have explored a range of values for γ_c from 2×10^{-2} to 2×10^2, and provide results for γ_c of 2×10^{-2}.

2.3 Results from the small scale model

Zones of localised deformation develop in the model, represented as planar distortions in the otherwise square grid (Fig. 3(b)) and also as zones roughly parallel to the shearing direction of alternating high and low shear stress (Fig. 3(c)). Histories were tracked of friction angle, the second invariant of the deviatoric stress tensor (the shear stress), and the second invariant of the deviatoric strain rate tensor (the strain rate) for three zones shown in Fig. 3(c) from different positions in the model. The resulting behaviours, patterns and magnitudes, were similar for the three zones (demonstrating the 'well behaved continuum behaviour' referred to in Appendix C, with deformation occurring in a coherent manner across adjacent zones). Figure 4 shows the behaviour of these 3 variables over 20000 numerical steps, within a total run of 3.1 million steps, equivalent to a model time of about 170 seconds. This takes about 45 hours running a Pentium 4 chip with a CPU of 3.20 GHz. Figure 5 shows the detailed behaviour of these 3 variables from a slightly later part of this time series, over just
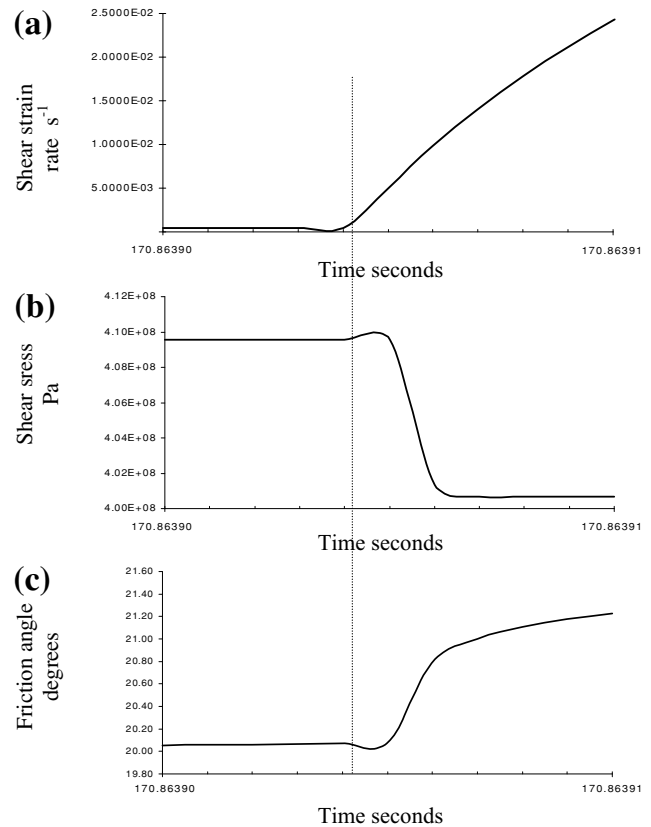

Fig. 5. Detailed behaviour over about 1.0e-5 seconds for zone Y in the simple shearing model shown in Fig. 3(c). a) Shear strain rate versus time. b) Shear stress versus time. c) Friction angle versus time.

1.0×10^{-5} seconds. There is a shear stress increase (approximately 1 MPa; Fig. 5(b)) accompanying the increase in shear strain rate following the stick-slip event (Fig. 5(a)), but instability in the system rapidly overtakes the stress evolution and drives it into a rapid stress drop of approximately 10 MPa. The friction angle (Fig. 5(c)) continues to evolve within this constrained system.

The stick-slip behaviour exhibited by these results provides a degree of validation as to the inclusion of rate and state dependant variable behaviour within a continuum formulation for an elastic-plastic material with cohesion.

Clearly, there is slightly different behaviour in each of the three zones shown in Fig. 3(c). Although these three zones occupy slightly different positions relative to the shear zones, it is not clear whether the different behaviours are related to these different deformation environments. To ascertain this, a much finer resolution model is needed, and this will be the subject of future work.

3. A Large Scale Model

3.1 Geological description

The particular model described here was developed in parallel with that described by Hobbs *et al.* (2004, this volume), and reflects interpretations of the Nagamichi-Rifu seismogenic fault in the Sendai region of NE Japan (Sato *et al.*, 2002). Discussions at the Sendai conference, the first of this series, focussed on processes operating at some depth corresponding to the base of the seismogenic zone (Ito *et*
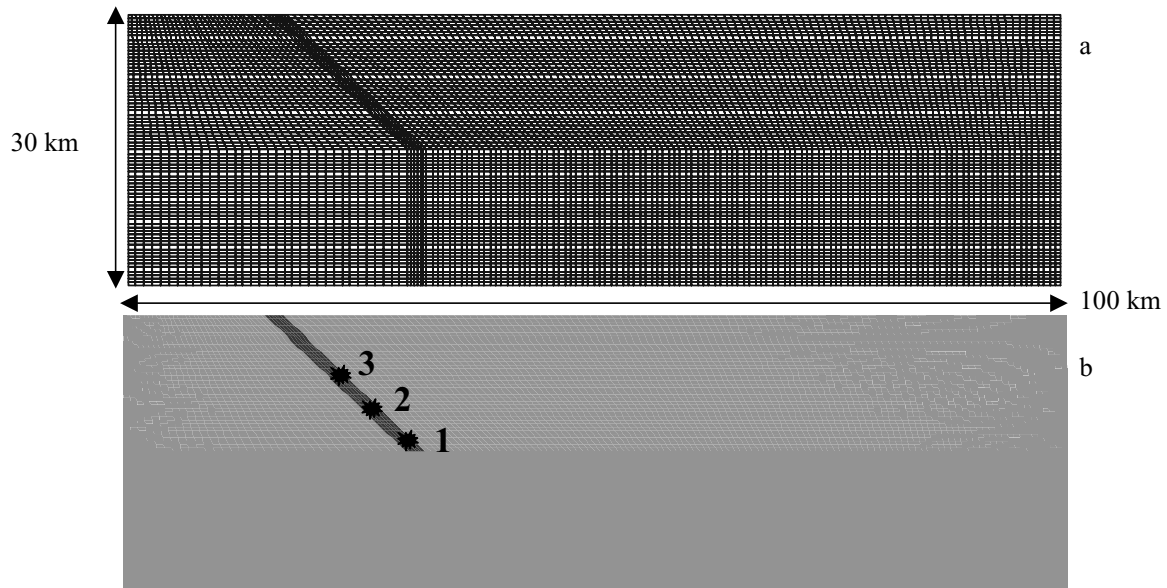
Fig. 6. a) Undeformed mesh for the crustal model. b) Position of region (dark grey) for which the rate and state dependant variable behaviour is applied. The markers, ✸, represent regions for which histories of variables are stored throughout the numerical experiments.

Table 3. Mechanical properties of the large scale crustal model.

Mechanical Property		
bulk modulus	4.7	GPa
shear modulus	2.8	GPa
density	2700	kg.m^{-3}
friction angle	30.0	degrees
initial friction angle within fault	25.0	degrees
dilation angle	1.0	degrees
cohesion	20.0	MPa
tensile strength	2.0	MPa

al., 2002), including the classical mechanism involving instability of frictional sliding in the brittle regime (Byerlee friction) for the production of large earthquakes at this depth (Hobbs *et al.*, 2002). This section extends these discussions through exploration of the application of rate and state dependant variable behaviour combined with elastic-plastic bulk material behaviour to the development and evolution of instabilities within a crustal-scale fault.

3.2   Computational model

As a first step, we choose a model 100 km long and 30 km deep for simulation of the Earth's crust (see Fig. 6(a) for computational grid). We assume at this stage that the material behaviour is temperature independent and has elastic-plastic rheology only. No fluids are present. The mechanical properties are assumed to be homogeneous, as a first step towards understanding the system, and are provided in Table 3. A shear zone is incorporated *a priori* into the model; it dips at 45 degrees from the ground surface down to 15 km depth and is 1.4 km thick. The fault has the same mechanical properties as the surrounding material except for the friction angle, which is initially 25 degrees; this

means the fault has a lower yield stress than the surrounding material. The friction angle of each zone within the fault changes continuously throughout the model with the application of the rate and state dependant variable behaviour shown in Table 2.

Gravity is applied to the model. The lower horizontal surface is a roller boundary in the x direction, and the two vertical surfaces are roller boundaries in the z direction. The top surface is left free. A bulk horizontal shortening rate of about $2 \times 10^{-15}\mathrm{s}^{-1}$ is imposed through applying an horizontal velocity to each of the vertical boundaries. A lithostatic stress regime is initialised throughout the model, and the model is brought to a steady state under these boundary conditions (200,000 numerical steps). Similar damping conditions to the small scale shearing model were also imposed, and are considered in Appendix B.

The rate and state formulation used is the same as in the simple shearing model, with the same values for parameters as in Table 2. As a first exploration of the behaviour of the fault, this formulation was applied only to the dipping region described earlier, and only from 2.4 km beneath the ground surface down to 15 km depth. The friction angle for the material within this region was updated every step according to the above-described bulk rate and state dependant formulation.

3.3   Results for the crustal scale model

The following results are examples of the solution that we obtain with the specific boundary conditions and parameters that we have chosen for our analysis. Our goal for this contribution was to formulate a numerically sound description of a hybrid continuum-rate and state variable friction approach. We have not done an extensive parameter search for comparison with natural scenarios. This is clearly the next step after the initial successful formulation of the model. The following results therefore should not be compared one-on-one with nature. We feel that a careful
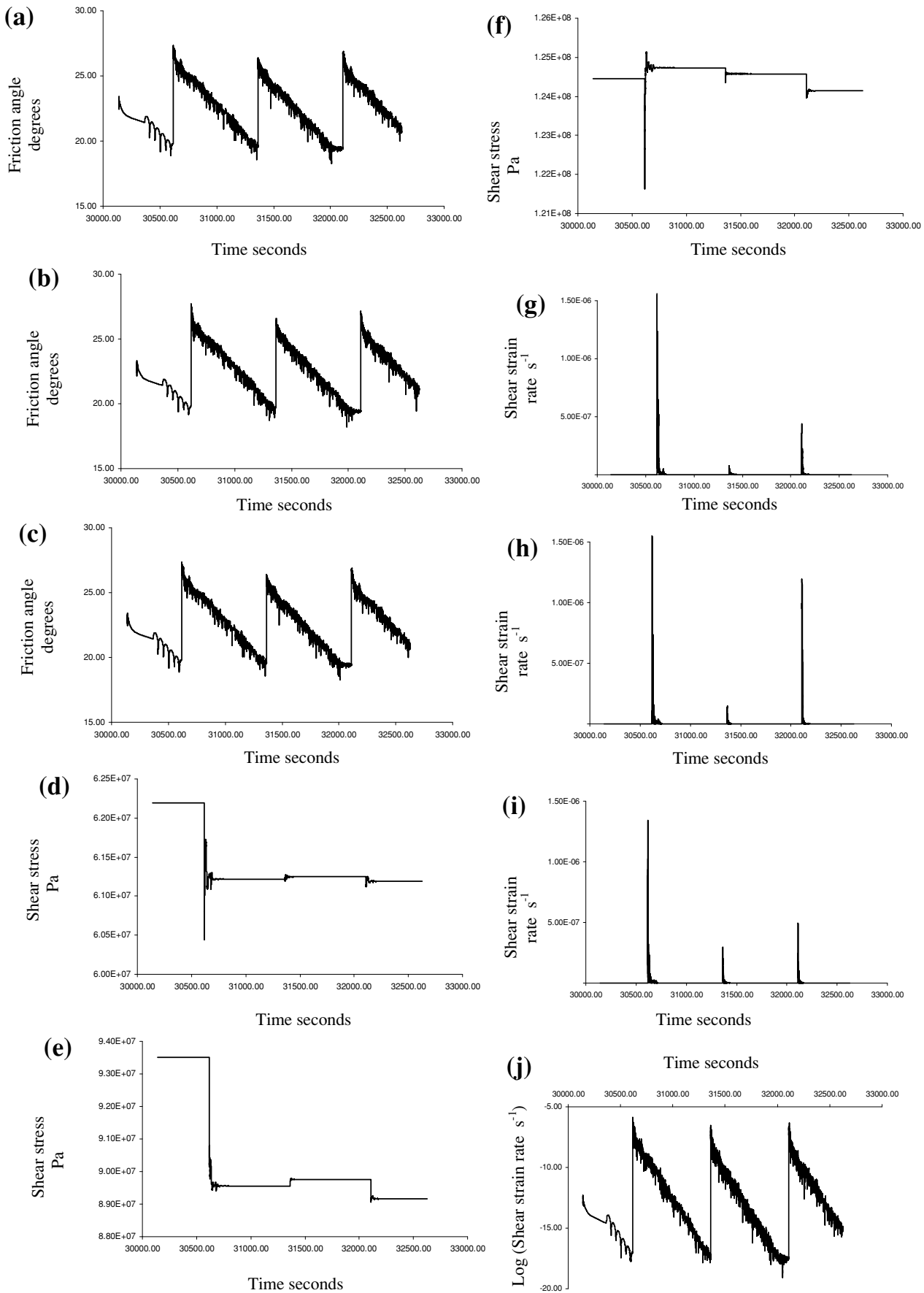
Fig. 7. Behaviour over 2500 seconds for the three zones shown in Fig. 6(b), in the crustal model. (a), (b), (c): Friction angle versus time. (d), (e), (f): Shear stress versus time. (g), (h), (i): Shear strain rate versus time. (a), (d), (g): Position 3 in Fig. 6(b). (b), (e), (h): Position 2 in Fig. 6(b). (c), (f), (i): Position 1 in Fig. 6(b). Figure 7(j) is a re-plot of Fig. 7(i), but now the logarithm of the shear strain rate is plotted against time. Notice the strong resemblance to Fig. 7(c).
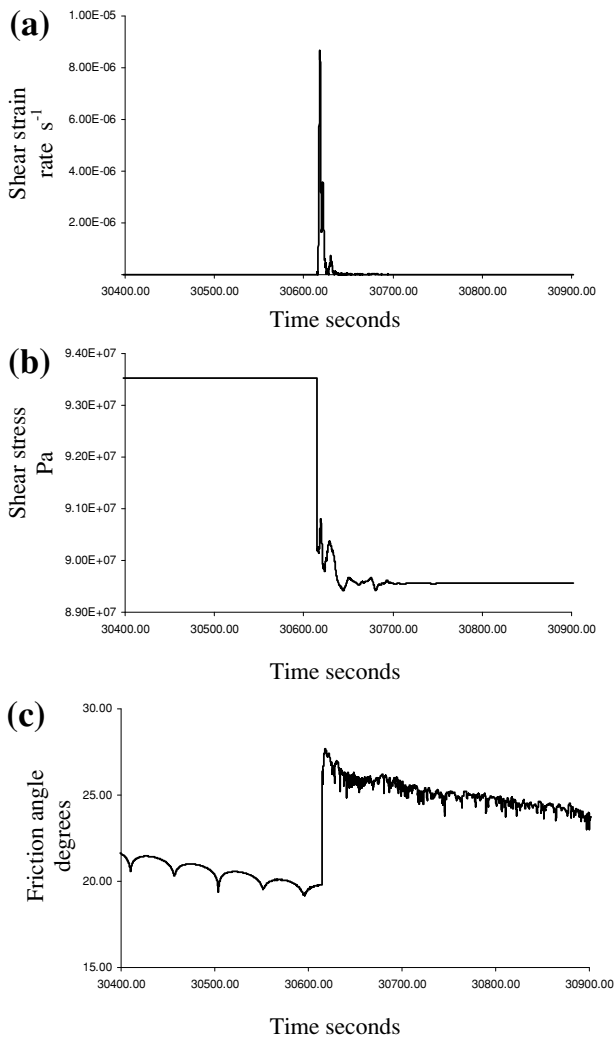
(a)

(b)

(c)

Fig. 8. Detailed behaviour over about 500 seconds for the first event in Fig. 7(h) for zone 2 in the crustal model shown in Fig. 6(b). a) Shear strain rate versus time. b) Shear stress versus time. c) Friction angle versus time.

discussion of the basic features of our smeared continuum method is warranted first.

Histories were collected continuously of the friction angle, shear stress, and strain rate for 3 zones at different depths within the fault region, originally at positions 6.3 km (point 3), 10.3 km (point 2), and 14.2 km (point 1) beneath the surface, as shown in Fig. 6(b). We show here just three unstable events (Fig. 7), occurring in a continuing numerical run. The zonal stick-slip behaviour described above occurs within these events, and is described in detail for the first event occurring at 10.3 km, in Fig. 8.

A zone situated near the middle of the fault (point 2 at 10.3 km in Fig. 6(b)) demonstrates behaviours similar to those described above for the simple shearing model: Stick-slip in the shear strain rate (Fig. 8(a)) is accompanied by a stress drop of 3.5 MPa (from 93.5 to 90.2 MPa; Fig. 8(b)) and an instantaneous increase in the friction angle (Fig. 8(c)), followed by a gentle decrease. In this case, the rapid rise and fall of the strain rate (Fig. 8(a)) is followed by a less abrupt increase and decrease also in the strain rate. The stress drop occurs over only 0.05 seconds (Fig. 8(b)).

Figure 7 shows that this behaviour of the strain rate at 10.3 km depth (Fig. 7(b)) appears to be reflected by zones both lower, at 14.2 km (Fig. 7(c); point 1, Fig. 6(b)), and higher in the crust, at 6.3 km (Fig. 7(a); point 3, Fig. 6(b)). It appears that instability is nucleated simultaneously at all three points in the fault.

4. Discussion

We have shown in this paper that the incorporation of a "smeared" rate and state formulation of friction evolution into otherwise bulk Mohr-Coulomb elastic plastic constitutive behaviour is capable of generating unstable behaviour within deforming fault gouge. This behaviour is identical to that demonstrated in other applications of rate and state dependant constitutive behaviour to discrete sliding surfaces (e.g. Tse and Rice, 1986; Lorig and Hobbs, 1990) in that an unstable event is accompanied by a stress drop, frictional evolution, and stick-slip behaviour. As indicated above, this approach is equivalent to the introduction of smeared damage mechanics into continuum codes (Lyakhovsky, 2001; Lyakhovsky *et al.*, 2001). Again, as with other numerical studies of unstable sliding of discrete surfaces the recurrence time between unstable events seems to be controlled by the elasticity of the system, as discussed by Rice (1983), Rice and Tse (1986), and by Tse and Rice (1986), and is dramatically short in comparison to recurrence times on natural faults. Various attempts have been made to address this problem with possible solutions including thermal pressurization (Sibson, 1973; see Noda and Shimamoto, 2004, for a review) and various aspects of melt generation (see Hirose and Shimamoto, 2004, for a review) with various degrees of success. An interesting alternative to the introduction of increasingly complex mechanisms has been explored by Iio (2004, this volume) in the form of feedback coupling between far-field sliding on a subduction zone through a viscous lower crust. This approach replaces the crust with a system of elastic springs, frictional sliders and dashpots (Fig. 1) and provides the opportunity for strong instantaneous (elastic) and long-term (viscous) feedback interactions between various parts of the crust. These types of coupled mechanical systems are more realistic representations of the crust than simple spring slider systems; they show considerable promise and are the subject of future work.

Experimental work by Shimamoto (1986), and Chester and Higgs (1992) has shown that even for a material that exhibits velocity weakening at a velocity $v = v_1$, that material may evolve at velocities greater than v_1 to exhibit velocity strengthening behaviour. This evolution in frictional behaviour is particularly appealing because it supplies a mechanism of inhibiting unstable slip once it has been nucleated at velocity v_1. Such behaviour may also be important in enabling relatively long recurrence times between unstable events and this issue should also be the subject of future work.

5. Conclusions

Modelling the behaviour from continuum to discrete deformation and from quasistatic to fully dynamic behaviour is one of the great challenges in the Geosciences. Several approaches have been proposed but none has been able fully

to reproduce the patterns observed in nature. This contribution provides some encouraging results for future analyses, particularly in investigation and comparison of two end-member approaches: one in which the best empirical data are combined to reproduce the basic phenomenon of earthquakes (this paper belongs to this class) and the other where earthquakes are simulated by an 'ab initio' approach avoiding, if possible, any empirical description. A novel computational method for understanding the mechanisms of earthquakes should be devised as a result of comparison of these two end members.

In this approach rate and state variable behaviour has been incorporated into a bulk constitutive model and applied to prediction of unstable behaviour in a homogeneous crustal model. Since in the second model described here, all 30 km thickness of crust was assumed to be represented by an elastic-plastic Mohr-Coulomb behaviour; there was no possible feedback between an upper elastic-plastic crust, and a lower viscous crust. It is suggested that such coupling and feedback is a requirement before geologically realistic recurrence times for instabilities may be attained, and before physically realistic energies are involved during the co-seismic slip periods. Future work based on this approach should include coupling with fluid flow, and exploration of the behaviour of fluid flow through the crust associated with faulting and earthquakes, leading to improved understanding of the feedback between earthquakes, faulting, and fluid flow.

Appendix A. Numerical Technique

Modelling of frictional sliding between two surfaces has been noted by Aagaard *et al.* (2001) to have been addressed in two distinct ways, through exploring the evolution of stress on the fault, and through modelling the rupture behaviour during earthquakes. Formulation of the rate- and state-dependant models (see review by Marone, 1998) has evolved through research on the former topic, while work on the latter topic has included either slip-weakening, or a combination of slip-weakening and rate-weakening behaviour. Incorporation of rupture dynamics in simulations of earthquakes and related processes has been explored in detail by many researchers including Tse and Rice (1986), Horowitz and Ruina (1989), Rice (1993), Cochard and Madariaga (1994), Ben-Zion and Rice (1995), Ben-Zion (1996), Cochard and Madariaga (1996), Rice and Ben-Zion (1996), Ben-Zion (2001), and Rice *et al.* (2001).

Advances in computer chip technology as well as in computational architectures and languages have allowed more efficient and faster computational modelling. Aagaard *et al.* (2001) note the increase in researchers using finite element, finite difference, and boundary integral methods with which to explore dynamic rupturing, moving into three dimensions.

Research has also addressed the incorporation of friction laws into continuum approximations supposing steady-state. In this case, Amontons' law is incorporated into the continuum formulation, with allowance made for time-dependence of frictional strength through an arbitrary strain-rate softening coefficient (Neumann and Zuber, 1995; Behn *et al.*, 2002), using a Lagrangian visco-plastic finite element model.

In this paper, allowance is made for rate- and state-dependence of the frictional strength. An explicit, finite difference program is used (Fast Lagrangian Analysis of Continua, FLAC) to explore this non-linear, dynamic behaviour. The numerical formulation is described in detail in the Users Handbook for FLAC (ITASCA, 2002). In summary, the approach is conceptually similar to that of dynamic relaxation (proposed by Otter *et al.*, 1966), with adaptations for arbitrary grid shapes and large-strains; the finite difference scheme follows the approach of Wilkins (1964). In the finite difference method (see for example Desai and Christian, 1977), every derivative in the set of governing equations is replaced directly by an algebraic expression written in terms of the field variables (e.g. stress or displacement) at discrete points in space; these variables are undefined within elements. The full dynamic equations of motion are included in the formulation with the aim of ensuring that the numerical scheme is stable when the physical system being modelled is unstable. Inertial terms are included and kinetic energy is generated and dissipated, with the influences of such energy generation and dissipation on the solution fully taken into account.

The general calculation procedure (ITASCA, 2002) first invokes the equations of motion to derive new velocities and displacements from stresses and forces. Second, strain rates are derived from velocities, and new stresses from strain rates. One timestep is taken for one full computational cycle. A timestep is chosen which is sufficiently small that information cannot physically pass from one element to another in that interval. Disturbances propagate across several elements only after several cycles. The aim is to ensure that the calculational 'wave speed' always keeps ahead of the physical wave speed. The stability condition for an elastic solid discretized into elements of size Δx is

$$\Delta t < \Delta x / C$$

where C is the maximum speed at which information can propagate, typically, the p-wave speed, C_p, where

$$C_p = ((K + 4G/3)/\rho)^{0.5} \qquad \text{(see Jaeger, 1969).}$$

Here K is the bulk elastic modulus, G is the shear elastic modulus, and ρ is the density.

Given the parameters for both models described here, for the small scale model, the primary wave velocity is $C_p = 5589$ m.s^{-1} and the shear wave velocity is $C_s = 3220$ m.s^{-1}; for the large scale model, the primary wave velocity is $C_p = 1767$ m.s^{-1} and the shear wave velocity is

$C_s = 1018$ m.s^{-1}. This implies that for a typical time step of 0.000125 seconds, as in the small scale model, the *p*-wave travels 0.7 metres and the *s*-wave travels 0.4 metres. Similarly, for a typical time step of 0.05 seconds, as in the large scale model, the *p*-wave travel 89 metres and the *s*-wave travels 51 metres. The element size is always 1 metre in the small scale model, and is always larger than 100 metres in the large scale model so that the above condition, that more than one step is always needed to propagate information across an element, is always satisfied.

The program performs a 'Lagrangian' analysis in that coordinates are updated at each timestep in large-strain mode; the incremental displacements are added to the coordinates so that the grid moves and deforms with the material it represents.

Appendix B. Dynamic Damping

For a dynamic analysis, the damping in the numerical simulation should reproduce in magnitude and form the energy losses in the natural system when subjected to a dynamic loading. What is normally attempted in a dynamic analysis is the reproduction of the frequency-independent damping of materials, particularly geological materials (Biggs, 1964; Cundall, 1976) at the correct level. However, in analyses that use a plasticity constitutive model such as Mohr-Coulomb, a considerable amount of energy dissipation can occur during plastic flow. Thus, for many dynamic analyses that involve large-strain, only a minimal percentage of damping (e.g. 0.5%) may be required. Further, dissipation will increase with amplitude for stress/strain cycles that involve plastic flow.

For dynamic calculations, a certain fraction of critical damping is usually required over a given frequency range. This type of damping is known as Rayleigh damping, where the fraction of critical damping operating at the centre frequency (in cycle/sec or Hertz) is input by the user. In this case, we used normal Rayleigh damping, and did not restrict the model to stiffness or mass-proportional damping.

As part of the dynamic analysis, quiet boundaries (that is, energy absorbing) were initially applied to the two vertical and lower horizontal boundaries. For reasons discussed below this approach was later abandoned. Numerical methods relying on the discretization of a finite region of space require that appropriate conditions be enforced at the artificial numerical boundaries. In static analyses, fixed or elastic boundaries can be realistically placed at some distance from the region of interest. In dynamic problems, however, such boundary conditions cause the reflection of outward propagating waves back into the model and do not allow the necessary energy radiation. The use of a larger model can minimize the problem, since material damping will absorb most of the energy in the waves reflected from distant boundaries. However, this solution leads to a large computational burden. The alternative is to use quiet (or absorbing) boundaries. The viscous boundary developed by Lysmer and Kuhlemeyer (1969) is used in this case. It is based on the use of independent dashpots in the normal and shear directions at the model boundaries (ITASCA, 2002).

The application of this approach proceeds by assuming first that the model has been brought to quasi-static equilib-

rium for the conditions of choice before the dynamic analysis is begun. In the case of the larger, crustal model, we are shortening the model using constant velocity boundary conditions on each vertical boundary. On initiation of the dynamic analysis, including application of the quiet boundaries, the code calculates the reaction forces obtained at the two vertical boundaries, and then replaces the applied velocity boundary conditions with equal and opposite reaction forces for the duration of the dynamic analysis. However, at least for the purpose of the crustal models run here, applying reaction forces instead of constant velocities at the boundaries leads to entirely the wrong result. The velocity boundary conditions appear to provide a driving force for the 'earthquake system' that is not sustained with the reaction force boundary conditions. Instead, in the latter case, as the model tends to equilibrium (remembering that the top surface is free to move), the forces in the model decrease and, as a consequence, in order to maintain the reaction forces at the boundary conditions, the code imposes higher and higher velocities. At the same stage in a number of models ($\sim 6 \times 10^5$ steps or $\sim 20 \times 10^3$ seconds), the variables which are being tracked by histories become completely stable, and remain stable out past 10^7 steps or 3×10^5 seconds. Quiet boundaries were therefore not applied for any further experiments. This approach worked also for the smaller, shearing model for which it was sufficient to initialize the velocity boundary conditions before beginning the dynamic analysis. We rely on material damping and the larger model for absorption of reflected energy.

Appendix C. Mesh Sensitivity

Rice (1993) was the first to focus on the dependence of the results of numerical simulations on cell, or computational grid, size, allowing for 'inherently discrete' fault models (fault models that have no well-defined continuum limit). Ben-Zion (2001) summarises the resulting research on the dependency of numerical results on the grid size, which occurs for simulations in which the assumed constitutive laws do not include a length scale over which material properties evolve, one example being the frictional law (Behn *et al.*, 2002). Further (see Ben-Zion, 2001), it is suggested by Rice and Ben-Zion (1996) that earthquake complexities observed from simulations with discrete and continuum systems (defined according to the success or otherwise of the coupling between the mathematical structures and the numerical calculations) are generated primarily by strong fault heterogeneities rather than any time-dependence of the system through quasi-static (Tse and Rice, 1986), quasi-dynamic (Rice, 1993; Ben-Zion and Rice, 1995), or fully dynamic (Rice and Ben-Zion, 1996: 'we have found no evidence that inclusion of fully inertial elastodynamics brings small event complexity of G-R (Gutenberg-Richter) type to our smooth fault models') simulations. Failure in a model may include the gradual and cooperative behaviour of many numerical cells (a well-behaved continuum behaviour); or failure may occur discontinuously with slip so that numerical zones may fail individually for any grid size (a poorly-behaved continuum behaviour, 'inherently discrete').

The models represented here exhibit continuum be-

haviour, according to this description, in that many numerical cells behave cooperatively, as shown in Figs. 4 and 7.

References

Aagaard, B. T., T. H. Heaton, and J. F. Hall, Dynamic earthquake ruptures in the presence of lithostatic normal stresses: Implications for friction models and heat production, *Bulletin of the Seismological Society of America*, **91**, 1765–1796, 2001.

Amontons, G., Histoire de l'Academie Royale des Sciences avec les Memoires de Mathematique et de Physique, 203–222, 1699.

Behn, M. D., J. Lin, and M. T. Zuber, A continuum mechanics model for normal faulting using a strain-rate softening rheology: Implications for thermal and rheological controls on continental and oceanic rifting, *Earth and Planetary Science Letters*, **202**, 725–740, 2002.

Ben-Zion, Y., Stress, slip, and earthquakes in models of complex single-fault systems incorporating brittle and creep deformations, *Journal of Geophysical Research*, **101**, 5677–5706, 1996.

Ben-Zion, Y., Dynamic ruptures in recent models of earthquake faults, *Journal of the Mechanics and Physics of Solids*, **49**, 2209–2244, 2001.

Ben-Zion, Y. and J. R. Rice, Slip patterns and earthquake populations along different classes of faults in elastic solids, *Journal of Geophysical Research*, **100**, 12,959–12,983, 1995.

Besuelle, P. and J. W. Rudnicki, *Localization: Shear Bands and Compaction Bands. Mechanics of Fluid Saturated Rocks*, edited by Y. Gueguen and M. Bouteca, International Geophysics Series, 89, Elsevier Academic Press, Amsterdam, 446 pp., 2004.

Biggs, J. M., *Introduction to Structural Dynamics*, New York: McGraw-Hill, 1964.

Borja, R. I. and A. Aydin, Computational modeling of deformation bands in granular media. I. Geological and mathematical framework, *Computer Methods in Applied Mechanics and Engineering*, **193**, 2667–2698, 2004.

Bowden, F. P. and D. Tabor, *The Friction and Lubrication of Solids, Part I*, Clarendon Press, Oxford, 1950.

Chester, F. M. and N. G. Higgs, Multimechanism friction constitutive model for ultrafine quartz gouge at hypocentral conditions, *J. Geophys. Res.*, **97**, 1859–1870, 1992.

Cochard, A. and R. Madariaga, Dynamic faulting under rate-dependent friction, *Pure and Applied Geophysics*, **142**, 419–445, 1994.

Cochard, A. and R. Madariaga, Complexity of seismicity due to highly rate-dependent friction, *Journal of Geophysical Research*, **101**, 25,321–25,336, 1996.

Cundall, P. A., Explicit finite difference methods in geomechanics, in *Numerical Methods in Engineering*, **1**, 132–150, 1976.

Desai, C. S. and J. T. Christian, *Numerical Methods in Geomechanics*, McGraw-Hill, New York, 783 pp., 1977.

Dieterich, J. H., Time-dependent friction and the mechanics of stick slip, *Pageoph*, **116**, 790–806, 1978.

Dieterich, J. H., Modelling of rock friction. Experimental results and constitutive equations, *J. Geophys. Res.*, **84**, 2161–2168, 1979.

Estrin, Y. and Y. Brechet, On a model of frictional sliding, *Pure and Applied Geophysics*, **147**, 745–762, 1996.

Gu, J.-C., J. R. Rice, A. L. Ruina, and S. T. Tse, Slip motion and stability of a single degree of freedom elastic system with rate and state dependent friction, *J. Mech. Phys. Solids*, **32**, 167–196, 1984.

Hirose, T. and T. Shimamoto, Growth of molten zone as a mechanism of slip weakening of simulated faults in gabbro during frictional melting, *J. Geophys. Res.*, 2004 (accepted).

Hobbs, B. E., H. Tanaka, and Y. Iio, Acceleration of slip motion in deep extensions of seismogenic faults in and below the seismogenic region, *Earth Planets Space*, **54**, 1195–1205, 2002.

Hobbs, B. E., A. Ord, K. Regenauer-Lieb, and B. Drummond, Fluid reservoirs in the crust and mechanical coupling between the upper and lower crust, *Earth Planets Space*, **56**, this issue, 1151–1161, 2004.

Horowitz, F. G. and A. Ruina, Slip patterns in a spatially homogeneous fault model, *J. Geophys. Res.*, **94**, 10279–10298, 1989.

Iio, Y., T. Sagiya, and Y. Kobayashi. What controls the occurrence of shallow intraplate earthquakes?, *Earth Planets Space*, **56**, this issue, 1077–1086, 2004.

ITASCA, FLAC, Fast Lagrangian Analysis of Continua, User's Guide, Version 4.00. ITASCA, Minnesota, USA, 2002.

Ito, H., G. Beroza, K. Fujimoto, and Y. Ogawa, Preface, *Earth Planets Space*, **54**, 999–100, 2002.

Jaeger, J. C., *Elasticity, Fracture and Flow*, Chapman and Hall, London, 268 pp., 3rd edition, 1969.

Lavenda, B. H., *Thermodynamics of Irreversible Processes*, Macmillan Press Ltd., London, 182 pp., 1978.

Lorig, L. J. and B. E. Hobbs, Numerical modelling of slip instability using the distinct element method with state variable friction laws, *Int. J. Rock Mech. Min. Sci. and Geomech. Abstr.*, **27**, 525–534, 1990.

Lyakhovsky, V., Scaling of fracture length and distributed damage, *Geophysical Journal International*, **144**, 114–122, 2001.

Lyakhovsky, V., Y. Ben-Zion, and A. Agnon, Earthquake cycles, fault zones, and seismicity patterns in a rheologically layered lithosphere, *Journal of Geophysical Research*, **106**, 4103–4120, 2001.

Lysmer, J. and R. L. Kuhlemeyer, Finite dynamic model for infinite media, *J. Eng. Mech.*, **95**, 859–877, 1969.

MacCurdy, E. da Vinci, L. Notebooks. Translation into English, Jonathan Cape, London, 1938.

Malvern, L. E., *Introduction to the Mechanics of a Continuous Medium*, Prentice-Hall, Inc., New Jersey, 713 pp., 1969.

Marone, C., Laboratory-derived friction laws and their application to seismic faulting, *Annu. Rev. Earth Planet. Sci.*, **26**, 643–696, 1998.

Neumann, G. and M. Zuber, A continuum approach to the develoment of normal faults, in Proc. 35th US Symposium on Rock Mechanics, Lake Tahoe, Nevada, edited by J. Daemen and R. Schultz, pp. 191–198, Balkema, 1995.

Noda, H. and T. Shimamoto, Thermal pressurization and slip-weakening distance of a fault: An example of the Hanaore fault, Southwest Japan, *Bull. Seism. Soc. Amer.*, 2004 (submitted).

Ord, A., Deformation of Rock: A pressure-sensitive, dilatant material, *Pure and Applied Geophysics*, **137**, 337–366, 1991.

Otter, J. R. H., A. C. Cassell, and R. E. Hobbs, Dynamic Relaxation, Paper No. 6986, *Proc. Inst. Civil Eng.*, **35**, 633–656, 1966.

Regenauer-Lieb, K. and D. Yuen, Positive feedback of interacting ductile faults from coupling of equation of state, rheology and thermal-mechanics, *Physics of Earth and Planetary Interiors*, **142**, 113–135, 2004.

Rice, J. R., Constitutive relations for fault slip and earthquake instabilities, *Pure and Applied Geophysics*, **121**, 443–475, 1983.

Rice, J. R., Spatio-temporal complexity of slip on a fault, *Journal of Geophysical Research*, **98**, 9885–9907, 1993.

Rice, J. R. and Y. Ben-Zion, Slip complexity in earthquake fault models, *Proc. Natl. Acad. Sci. USA*, **93**, 3811–3818, 1996.

Rice, J. R. and S. T. Tse, Dynamic motion of a single degree of freedom system following a rate and state dependent friction law, *Journal of Geophysical Research*, **91**, 521–530, 1986.

Rice, J. R., N. Lapusta, and K. Ranjith, Rate and state dependent friction and the stability of sliding between elastically deformable solids, *Journal of the Mechanics and Physics of Solids*, **49**, 1865–1898, 2001.

Ruina, A. L., Friction laws and instabilities: a quasi-static analysis of some dry friction behaviour. Ph.D. thesis, Division of Engineering, Brown University, 1980.

Ruina, A. L., Slip instability and state variable friction laws, *J. Geophys. Res.*, **88**, 10259–10270, 1983.

Sato, H., T. Imaizumi, T. Yoshida, H. Ito, and A. Hasegawa, Tectonic evolution and deep to shallow geometry of Nagamachi-Rifu active fault system, NE Japan, *Earth Planets Space*, **54**, 1039–1043, 2002.

Shimamoto, T., Transition between frictional slip and ductile flow for halite shear zones at room temperature, *Science*, **231**, 711–714, 1986.

Sibson, R. H., Interactions between temperature and pore-fluid pressure during earthquake faulting and a mechanism for partial or total stress relief, *Nature Physical Science*, **243**, 66–68, 1973.

Tse, S. T. and J. R. Rice, Crustal earthquake instability in relation to the depth variation of frictional slip properties, *Journal of Geophysical Research*, **91**, 9452–9472, 1986.

Vermeer, P. A. and R. de Borst. Non-associated plasticity for soils, concrete and rock, *Heron*, **29**, 3–64, 1984.

Wilkins, M. L. Calculation of elastic-plastic flow, in *Methods in Computational Physics, 3, Fundamental Methods in Hydrodynamics*, pp. 211–263, edited by Alder, New York: Academic Press, 1964.

A. Ord (e-mail: Alison.Ord@csiro.au), B. E. Hobbs, and K. Regenauer-Lieb